Solar Energy Materials & Solar Cells 218 (2020) 110764

Contents lists available at ScienceDirect

Solar Energy Materials and Solar Cells

journal homepage: http://www.elsevier.com/locate/solmat

Semi-transparent p-type barium copper sulfide as a back contact interface layer for cadmium telluride solar cells

Kamala Khanal Subedi, Ebin Bastola, Indra Subedi, Sandip S. Bista, Suman Rijal, Manoj K. Jamarkattel, Rasha A. Awni, Adam B. Philips, Yanfa Yan, Michael J. Heben, Nikolas J. Podraza, Randy J. Ellingson *

Wright Center for Photovoltaic Innovation and Commercialization, Department of Physics and Astronomy, The University of Toledo, Toledo, OH, 43606, USA

ARTICLE INFO

Keywords:
Barium copper sulfide
Back contact
Bifacial
CdTe solar cell
Solution based method

ABSTRACT

Optically transparent p-type materials play a critical role in transparent electronics including photovoltaic (PV) devices. P-type sulfide materials offer an alternative to oxides for PV application due to improved hole transport properties. Here, we report the solution-based synthesis of earth-abundant p-type transparent conducting barium copper sulfide (α-$BaCu_4S_3$, BCS) thin films. These films were characterized using scanning electron microscopy, X-ray diffraction, UV–Vis–NIR spectrophotometry, Raman spectroscopy, and spectroscopic ellipsometry. BCS films of ~100 nm thickness transmit >70% of visible light. We report on tests of the hole transport properties of these BCS films for cadmium telluride (CdTe) photovoltaics, finding that the BCS deposition process forms a beneficial tellurium (Te) rich surface on CdTe by selectively removing Cd from the surface. Based on our study, the BCS interface layer plays dual functions for CdTe PV devices as a hole transport material and as an etchant, enhancing the resulting device performance. We observed a significant increase in open-circuit voltage of CdTe solar cells with the BCS buffer layer. Additionally, we discuss semitransparent CdTe solar cells with BCS as a hole transport layer and indium tin oxide as a finishing electrode. Semitransparent CdTe solar cells shows 13.3% conversion efficiency for the front side illumination and 1.2% efficiency for back side illumination, indicating high recombination of charge carriers generated close to the rear CdTe/BCS/ITO contact.

1. Introduction

Transparent conductors are an essential part of various electronic devices including solar cells, sensors, and transparent circuits [1,2]. All of the currently commercialized transparent conducting materials (TCMs) including Sn-doped In_2O_3(ITO) [3] and, F-doped SnO_2 (FTO) are n-type [4], and the availability of p-type materials with equivalent optical transparency and conductivity is limited. However, many efforts have recently been directed to the development of such p-type TCMs based on copper (Cu) compounds such as $CuAlO_2$ [5], $(CuS)_x$ $(ZnS)_{1-x}$ [6–8], and $BaCu_2S_2$ [9–11]. Optically transparent p-type conductors facilitate the development of transparent electronics as well as high efficiency bifacial photovoltaic devices [6]. According to theory, due to the tradeoff between the position of valence band maximum and forbidden bandgap, complex sulfide semiconductors could be interesting and appropriate candidates for p-type TCMs [12]. Complex sulfides can be formed by replacing the more ionic oxides with more covalent sulfides; this has led to the development of copper sulfide-based materials, including $CuAlS_2$ [13], $(CuS)_x$ $(ZnS)_{1-x}$ [6,7], $BaCu_2S_2$, and $BaCu_4S_3$ [11].

Among these sulfide materials, $BaCu_4S_3$ shows some preferable characteristics for practical applications like wider bandgap and high transparency in the visible to near infrared (NIR) spectral regions [14,15]. Limited studies have previously reported on p-type barium copper sulfide. For example, Han et al. reported sputtered $BaCu_4S_3$ thin films with p-type conductivity and carrier concentration $\sim 5 \times 10^{19}$ cm^{-3} [11], while Wang et al. used highly toxic anhydrous hydrazine as a solvent to fabricate p-type $BaCu_2S_2$ for their solution based process in an inert environment [10]. In this context, the development of an environmentally-friendly p-type BCS TCM via a low temperature, tunable, and scalable method is highly desirable. Our BCS thin films consist of non-toxic earth-abundant materials [16].

Due to the deep work function of CdTe (~5.7 eV), it is difficult to make an ohmic contact for hole extraction on the back interface of CdTe

* Corresponding author.
E-mail address: Randy.Ellingson@utoledo.edu (R.J. Ellingson).

https://doi.org/10.1016/j.solmat.2020.110764
Received 21 June 2020; Received in revised form 19 August 2020; Accepted 20 August 2020
Available online 8 September 2020
0927-0248/

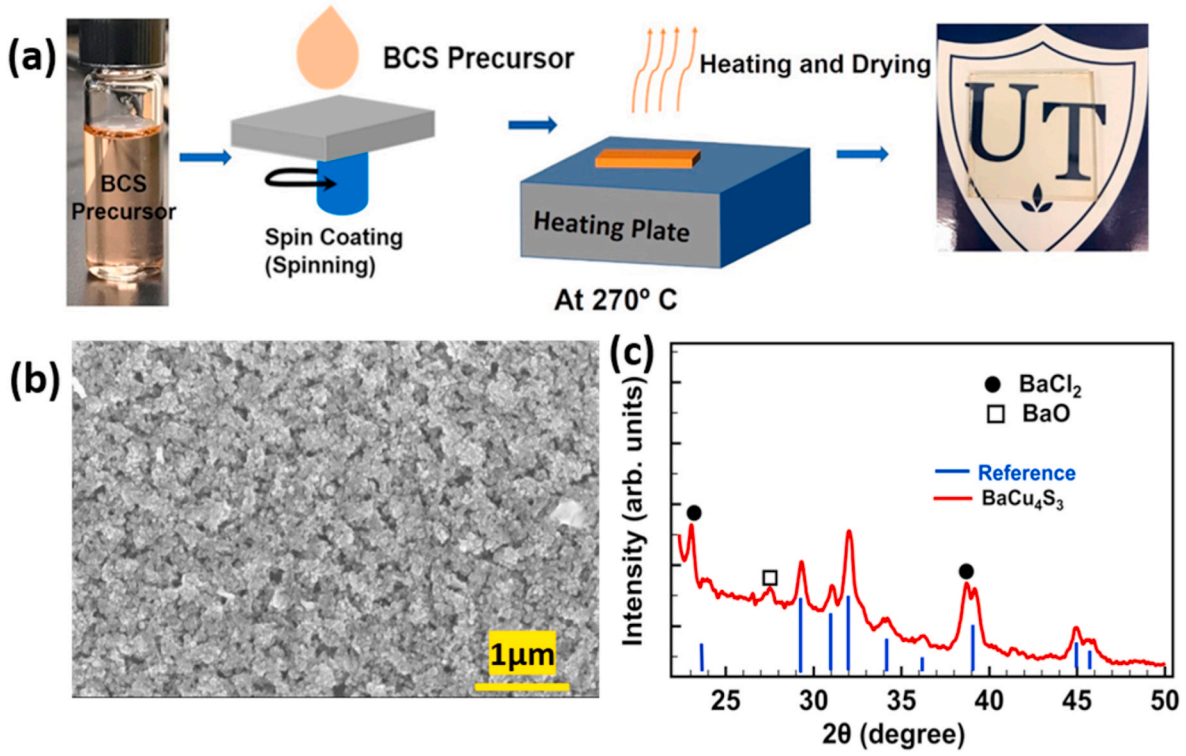

Fig. 1. (a) Synthesis process (b) plan-view scanning electron microscopy (SEM) images (c) X-ray diffraction (XRD) patterns where □ represents BaO and ● represents $BaCl_2$ (# PDF 97-000-2190) impurity phase of BCS nanocomposite thin films deposited on soda lime glass substrates.

solar cells. Copper/gold (Cu/Au) has been used as a back contact material for CdTe photovoltaics, though the existence of a Schottky potential barrier of ~0.330 eV limits device performance [17,18]. To improve the open-circuit voltage (V_{OC}), one common process is to introduce a back contact buffer layer with appropriate work function. There are many reports focusing on Cu containing interfacial layers such as copper-doped zinc telluride (ZnTe:Cu), Cu_9S_5, and iron pyrite (FeS_2) to reduce the back barrier height between the CdTe and standard back contact [19–21]. Other approaches include the formation or deposition of a tellurium (Te) layer on the back interface which reduces the back barrier height [22–24]. The back contact interface layer ideally facilitates hole transport towards the electrode while inhibiting electron transport to the back contact by creating an upward band bending for better device performance [25,26]. The desired hole transport properties for CdTe solar cells are p-type, low resistivity, and make the upward band-bending by creating a positive initial Fermi level offset (IFLO) [25,27]. Additionally, if these properties could be maintained while allowing high visible-to-NIR transparency in the hole transport materials, one could fabricate a bifacial device that efficiently converts incident solar irradiance from both front and rear contacts into electrical power. Although bifacial architecture is common for crystalline silicon solar cells, there are few examples of studies that contribute to bifacial thin film solar cell technology [7,29,31].

In this work, we report the fabrication and characterization of $BaCu_4S_3$ (BCS), a wide bandgap, transparent p-type semiconductor, thin films by using a low temperature solution based method. Our initial results with BCS/ITO as a transparent back electrode showed promising results for vapor transport deposition (VTD) deposited CdTe for through the glass illumination of transparent solar cells [15]. Here, we have extended our work to study opaque back contact configurations for both VTD and close space sublimation system (CSS). Our study also reports on semitransparent CSS deposited CdTe solar cells, and we have applied detailed characterization including spectroscopic ellipsometry (SE) to understand surface morphology, optical properties, and the dependence of performance on device structure. BCS films deposited to a thickness ~100 nm have a 1.92 eV bandgap energy and >70% transmittance in the visible to NIR spectral range. Due to its p-type conductivity, and high hole concentration, BCS films are evaluated as the hole transport properties for CdTe photovoltaics. Based on our study, BCS works very well as a hole transport layer for CdTe with Au as a metallization layer, resulting in a significant increase in V_{OC}. Our best devices for VTD CdTe yielded a high Voc of 839 mV, fill factor of 75%, and 14.4% power conversion efficiency with BCS as buffer layer between the CdTe and Au. This provides a 7.5% relative efficiency improvement over a device with a standard Cu/Au back contact layer. Furthermore, for a semi-transparent bifacial device design using BCS/ITO as a buffer layer, from the glass side illumination we observed an increase in V_{OC} to 836 mV and overall device performance comparable to our control device. However, the BCS/ITO back contact exhibits very low current-density through contact (back) side illumination, limiting the conversion efficiency to 1.2%. We also address the performance under back-side illumination, where the external quantum efficiency (EQE) is limited due to the high surface recombination between the CdTe and BCS/ITO interface.

2. Experimental details

2.1. Chemicals

Copper (II) chloride ($CuCl_2$), barium acetate (Ba $(CH_3COO)_2$) thiourea (CH_4N_2S), lactic acid ($C_3H_6O_3$), and 2-methoxyethanol ($C_3H_8O_2$) were purchased from Fisher Scientific and acetylacetone ($C_5H_8O_2$) was bought from Sigma Aldrich. No further purification is done on these chemicals and all stored at room temperature.

2.2. Preparation and device fabrication

The glass substrate cleaning and precursor making process is followed from our recently published work [15]. However, the concentration of these precursor is modified here. Solution I contain Cu–S made by dissolving 0.4 M $CuCl_2$ with 1.23 M CH_4N_2S into 2 mL 2-methoxyethanol and 3–4 drops of acetylacetone while solution II consists of 0.4 M barium acetate dissolved into 1 mL 2-methoxyethanol with 6–7 drops of lactic acid. To prepare BCS thin films and back buffer layer on CdTe, 50 μL BCS precursor solution was placed on the substrate, spin at 3500 rpm for 55 s after pre-spin at 1000 rpm for 10 s and annealed at 270 °C for 5 min.

The solar cell film stack layers (CdS/CdTe, with CdS = 120 nm and CdTe = 3.2 μm) were deposited by VTD and obtained from Willard and Kelsey Solar Group. We also utilized CdTe devices fabricated via CSS with oxygenated CdS (CdS:O) as the window layer. The CdS/CdTe film stacks were treated with a saturated $CdCl_2$ solution in methanol, annealed at 387 °C for 30 min in dry air. Subsequently, the BCS HTL layer were deposited onto $CdCl_2$-treated CdS/CdTe devices as the HTL. After depositing HTL layer and post annealing process, some impurities of $BaCl_2$ formed during the preparation of BCS layer were removed by rinsing the film stack in methanol [32]. After the methanol rinse, there is no $BaCl_2$ present on the CdTe surface as verified by the XRD measurement. Finally, a 40 nm Au layer was thermally evaporated to complete the back contact, and 532 nm laser scribing defined approximately 20 cells, each with an active device area of 0.06 cm^2.

The ITO was sputter-deposited at room temperature at 2 mTorr Ar pressure and 120 W power for 90 min. These semitransparent film stacks were scribed mechanically to produce the groups of cells with active area 0.08 cm^2.

2.3. Characterization

The surface and cross-sectional morphologies of BCS films were studied by using Hitachi S-4800 UHR scanning electron microscope (SEM). Elemental composition by energy dispersive X-ray spectroscopy (EDS) operated at 20 kV, and 10 μA. The X-ray diffraction (XRD) measurement is done by a Rigaku Ultima III X-ray Diffractometer where used accelerating voltage and currents were 40 kV and 44 mA, respectively. Unpolarized optical parameter were studied by using a PerkinElmer Lambda 1050 UV/Vis/NIR spectrophotometer. Raman spectra were measured by using 632.8 HeNe laser. Ex situ spectroscopic ellipsometry data of barium copper sulfide (BCS) thin films deposited on soda lime glass have been collected at 50°, 60°, and 70° angles of incidence at room temperature using a single rotating compensator multichannel ellipsometer [31,32]. Spectral range is varied from 0.735 to 5.887 eV (M-2000FI, J.A. Woollam Co.).

Current density vs. voltage ($J-V$) characteristics and external quantum efficiency (EQE) measurement is done by using a Keithley 2440 digital source meter with a LED solar simulator (MiniSol model LSH-7320) and PV Instruments (model IVQE8-C) system respectively.

3. Results and discussion

The synthesis process of BCS films on the glass substrate is shown in Fig. 1(a). The surface morphology of the BCS films on the glass substrate as obtained by plane view SEM is shown in Fig. 1(b). The composition of the Ba: Cu: S is found to be ~1:4:3 (see Fig. S1). Similarly, The XRD pattern in Fig. 1(c) indicates that the BCS thin film exhibits an orthorhombic α-phase crystal structure (# PDF 98-001-9167) [10]. The maximum transmittance of >70% was obtained within the 400–900 nm wavelength range [15]. The band gap energy of BCS film is found to be (1.92 ± 0.05) eV as determined by a Tauc plot where the absorption coefficient has been obtained from the unpolarized transmittance spectra using Beer's Law [33], which is in agreement with that measured for a sputtered BCS film by Han et al. [11]. The sheet resistance of these BCS films was found to be high, on the order of 10^6 -10^7 Ωsq^{-1} due to high surface roughness, and low mobility. Additionally, we were not able to carry Hall effect measurements to estimate the carrier concentration; the resistive nature and unknown Fermi level of this material presented practical challenges for preparation of an ohmic contact.

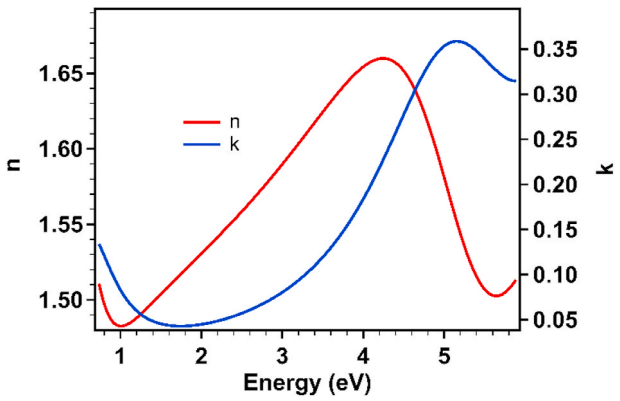

Fig. 2. Complex index of refraction ($N = n + ik$) for a BCS film on soda lime glass as measured by spectroscopic ellipsometry (SE).

The complex optical properties in the form of the complex dielectric function ($\varepsilon = \varepsilon_1 + i\varepsilon_2$) or complex index of refraction ($N = n + ik = \varepsilon^{1/2}$) spectra for a BCS film is determined from analysis of measured ellipsometric spectra. Ellispometric spectra are measured at three angles of incidence (50°, 60°, and 70°). SE data from all three angles have been fit simultaneously to structural and optical models using a least square regression and an unweighted error function, σ [34]. The structural model used for SE data analysis consists of semi-infinite soda lime glass substrate/BCS thin film/surface roughness/air ambient. The complex optical properties of the BCS film are modeled by using a constant additive term to ε_1 denoted as ε_∞, a Sellmeier expression, and three Lorentzian oscillators [35]:

$$\varepsilon(E) = \varepsilon_\infty + \frac{A_s}{E_s^2 - E^2} + \sum_{m=1}^{3} \frac{A_m \Gamma_m E_m}{(E_m^2 - E^2) + i\Gamma_m E} \quad (1)$$

For each Lorentz oscillator (m), A_m is the amplitude, E_m is the resonance energy, and Γ_m is the broadening. Similarly A_s and E_s are amplitude and resonance energy for the zero-broadened Sellmeier expression. The optical properties of the surface roughness layer are modeled by using a Bruggeman effective medium approximation consisting of variable fractions of the complex optical properties of the BCS film and void [36,37]. Reference optical properties of soda lime glass substrate are from the Junda et al. [38]. Optical properties in the form of spectra in complex N are shown in Fig. 2.

The bulk film thickness is found to be 47 ± 6 nm, and surface roughness thickness is 39 ± 5 nm. The surface roughness layer consists of 0.079 ± 0.004 void fraction and 0.921 BCS. The substantial surface roughness layer thickness is likely due to the film structure having small grains without complete contact as seen from the SEM. Low photon energy absorption observed with increasing values of k at decreasing photon energy may be due to the presence of other phases, multiple copper valence states, phonon modes, free carrier absorption, or a combination of these effects [39]. The model fit parameters are reported in Table S1(SI).

To study the hole transport properties of these BCS film, we deposited a BCS layer on the back of the CdTe PV filmstack. The transmission spectra with BCS and ITO back contact is shown in Fig. S2. Fig. 3(a) and **(b)** shows the SEM images of CdTe films without and with BCS layer, respectively. After BCS layer deposition on CdTe, the surface shows some grains of BCS along with Te islanding. EDS measurement of the CdS/CdTe film stack with BCS back buffer layer is shown in Fig. S3. The

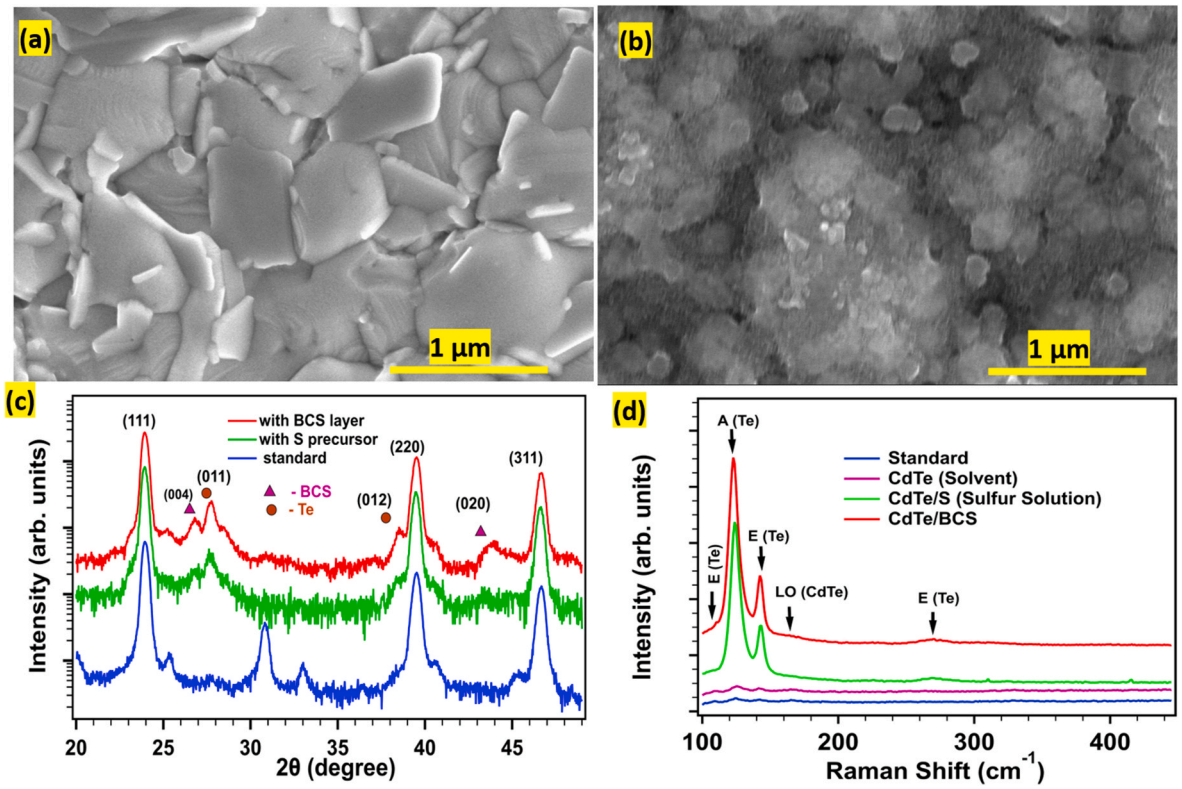

Fig. 3. SEM of (a) surface morphology of a VTD CdTe film and (b) a CdTe film after BCS deposition, (c) XRD patterns of CdTe with and without BCS, and for a sulfur precursor treated CdTe film, and (d) Raman spectra of VTD deposited CdTe surface with or without BCS layer using 632.8 nm excitation from a HeNe laser.

variation in the stoichiometry of atoms is nearly the same as for the BCS film deposited on the soda lime glass. XRD measurement shows the Te peak after deposition of BCS on CdTe. The SEM image for a device treated with sulfur precursor (dissolving thiourea into 2-methoxyethanol) followed with post annealing treatment is shown in the SI (Fig. S4). The three predominant diffraction peaks at position (in 2θ) of 23.8°, 39.3°, and 46.4° of Fig. 3 (c) correspond to the cubic CdTe [40]. The peaks at 27.5° and 38.5° correspond to (011) and (012) planes of Te respectively. At the same time, we observed peaks from BCS layer corresponding to the peak positions (2θ) 26.4° and 44.8° confirming the presence of $BaCu_4S_3$ on the CdTe surface. The CdTe surface was measured by Raman spectroscopy to confirm the presence of Te after BCS deposition. Laser can have an effect on the CdTe surface to make it Te rich [41]. Thus, to minimize the effect of the laser, we exposed the sample for no more than approximately 30 s. Fig. 3(d) displays the Raman spectra of the CdTe surface with and without BCS layer and treated with solvent only and with S- precursor (thiourea complex). We clearly observed strong Te vibrational peaks at 123, 143, 266 cm^{-1} on CdTe surface with either BCS thin film or simply following the S precursor anneal. At 270 °C thiourea starts to form a thiourea-metal complex, in this case via metal complexings with Cd to yield a Te rich surface [42,43]. Further, these measurements were made under identical conditions to have minimal effect of the laser on CdTe surface. The peak at 123 cm^{-1} is due to the A (Te) mode, and the other peaks at 143, 260 cm^{-1} are likely due to the E (Te) vibration modes [44,45], and the peak at 165 cm^{-1} is for standard CdTe [46]. However, peak intensity LO (CdTe) is lower than others, so it is not clearly discernible in Fig. 3(d). Slight variation of the peak positions of A (Te) between standard, S-precursor, and BCS on CdTe surface due to the tensile stress in thin film [47].

Fig. 4(a) below displays a schematic diagram and cross-sectional micrograph of CdS/CdTe solar cells. The thickness of the BCS films on the CdTe is ~100 nm based on the SEM image, and it is also verified by using ImageJ software measurement [48]. Fig. 4(b) shows the *J-V* curve of the best cells among 20 cells of each contact type. The solid lines represent measurements under simulated AM1.5G illumination, and dotted lines represent dark measurements. Average values for open circuit voltage (V_{OC}), short circuit current density (J_{SC}), fill factor (*FF*), efficiency (η), series resistance (R_S), and shunt resistance (R_{Sh}) of the CdTe device with BCS/Au, Au, and Cu/Au contacts are shown in Table 1. From the introduction of the BCS buffer layer between the CdTe and Au, the V_{OC} increase was substantial from 806 to 839 mV and *FF* was also improved from 73.3 to 75.0%. The relative increase of device performance efficiency in comparison with the Cu/Au contact is ~7.5% with the excellent V_{OC} improvement whereas there is slightly improvement of J_{SC} of the device with novel BCS and standard Cu/Au back contacts. This improvement in V_{OC} and the absence of the rollover effect and reducing crossover effects suggest that BCS plays an important role as a back buffer layer on CdTe when completed with Au [49]. The EQE spectra shown in Fig. S5 confirm the J_{SC} values obtained from *J-V* measurements. The effect of etching with sulfur precursor on device performance with a standard Cu/Au contact is discussed in the SI (Fig. S6 and Table S2). Further, we tested these BCS interface layers in CdTe devices fabricated using CSS method and found consistent improvement (Fig. S7, Table S3).

Optical absorption properties evaluated by using the transmittance spectroscopy and SE shows the BCS film has high transmittance into the visible to NIR spectral region. This indicates that BCS could serve as a transparent back buffer layer for semi-transparent CdTe solar cells. Bifacial PV cell configuration requires a p^+ type transparent hole transport material because the barrier height between CdTe and ITO is problematic, yielding inefficient tunneling as the most probable mechanism for the hole transport between CdTe and ITO [7,50]. Insertion of a thin p^+ layer between the CdTe and ITO can improve hole transfer from CdTe to the ITO [51,52], and our tested cells use CdTe/BCS/ITO. The

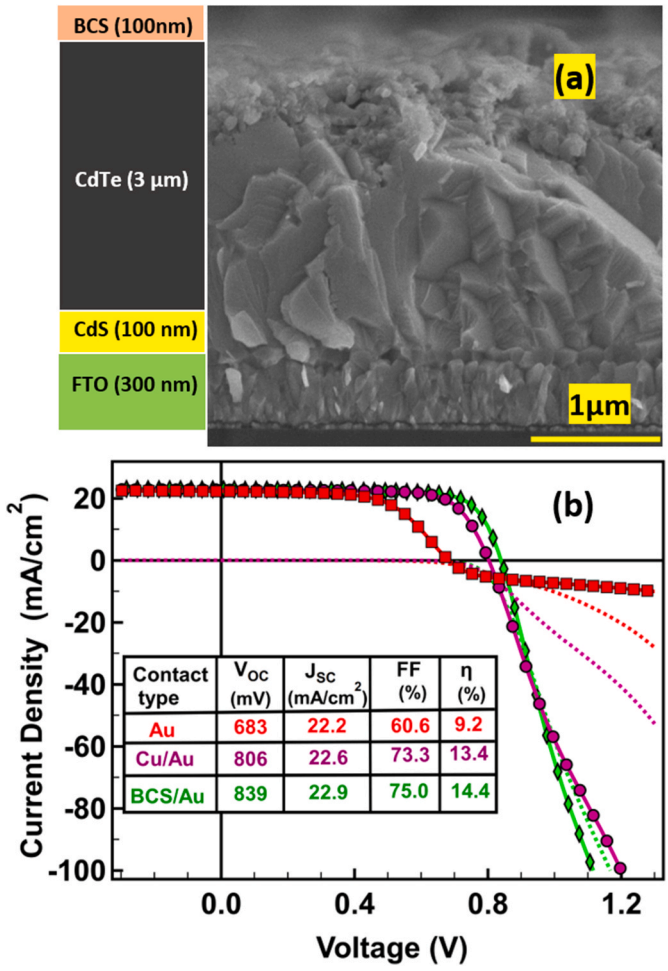

Fig. 4. (a) Schematic diagram and cross sectional SEM of a VTD deposited CdTe solar cell with BCS as HTL layer, and (b) *J-V* characteristics of CdS/CdTe solar cell devices with and without BCS thin films as interface layers.

interface between BCS and ITO creates a narrow depletion region and facilitates the hole transport through BCS to ITO. Furthermore, the back barrier height between the Te/ITO has been demonstrated as a low barrier for the entire device. CdTe/BCS device structure shows the Te rich surface which helps create a low barrier height resulting in good device performance for glass side illumination [15,22]. The device performance of CdTe/BCS/ITO from glass side and contact side illumination and comparison between the standard Cu/Au are shown in Fig. 5. It can be seen that introduction of the BCS layer at the interface between the CdTe and ITO shows the 13.3% device performance. The V_{OC} increased substantially from 793 to 836 mV; however, *FF* is decreased from 69.7% to 66.1% which could be due to series resistance of ITO (~25 Ω/sq), and J_{SC} remained similar for the BCS back contact as compared to the standard Cu/Au back contact. EQE measurement and average device performance of the device CdTe/BCS/ITO configuration with comparison of controlled sample is shown in the SI (Fig. S8 and Table S4).

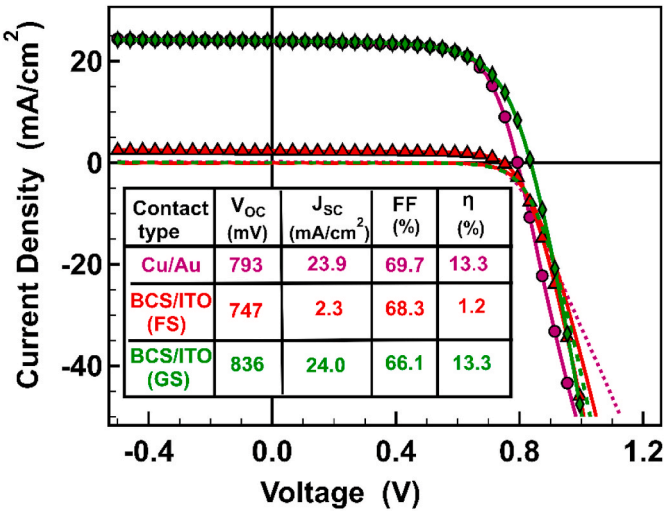

Fig. 5. *J-V* characteristics of CSS deposited CdTe solar cells, comparing the performance of a lab standard Cu/Au contact with front and back-illuminated semitransparent cells using BCS as a buffer layer.

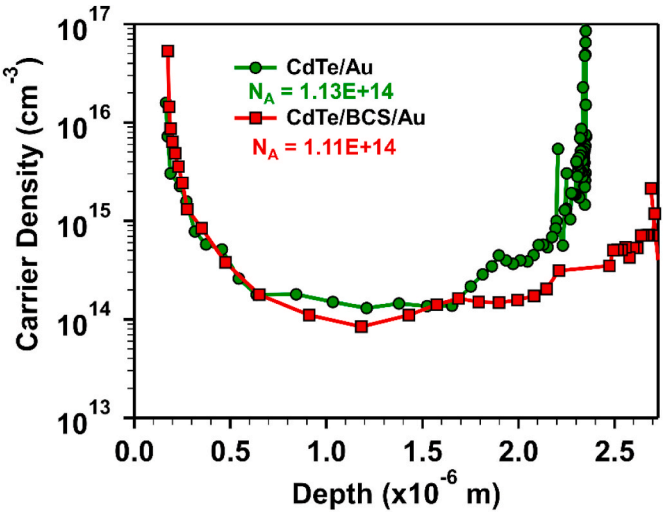

Fig. 6. C–V measurement used to determine the apparent carrier density of the CdTe film stack with BCS/Au and Au only interface layer.

The rear side illumination of the device is affected by high recombination loss due to the low diffusion length in CdTe, high surface recombination velocity, and can also be due to the downward band banding [25,53,54]. Photoelectrons generated near the back contact must travel to reach the front electrode so current density is reduced by the interface recombination. If we can passivate the interface by using chemical passivation to reduce the BSRV, or by field effect passivation to reduce the free electron concentration at the back contact, then we can improve the device performance from the backside [26]. And fabricate good bifacial devices and/or efficient tandem configurations. We use this result as an opportunity to illuminate the simultaneous need for

Table 1
Average device performance parameters along with their standard deviation of 20 cells for each back contact configuration.

Back Contact Types	Device Parameters					
	V_{OC} (mV)	J_{SC} (mA/cm^2)	*FF* (%)	PCE (%)	R_S (Ωcm^2)	R_{Sh} (Ωcm^2)
Au	647 ± 23	22.2 ± 0.2	62.3 ± 1.8	8.9 ± 0.4	7.0 ± 1.6	1671 ± 353
Cu/Au	806 ± 4	22.5 ± 0.2	73.0 ± 1.0	13.2 ± 0.2	3.6 ± 0.6	2603 ± 230
BCS/Au	841 ± 2	22.6 ± 0.3	73.7 ± 1.0	13.9 ± 0.6	2.8 ± 0.2	1866 ± 282

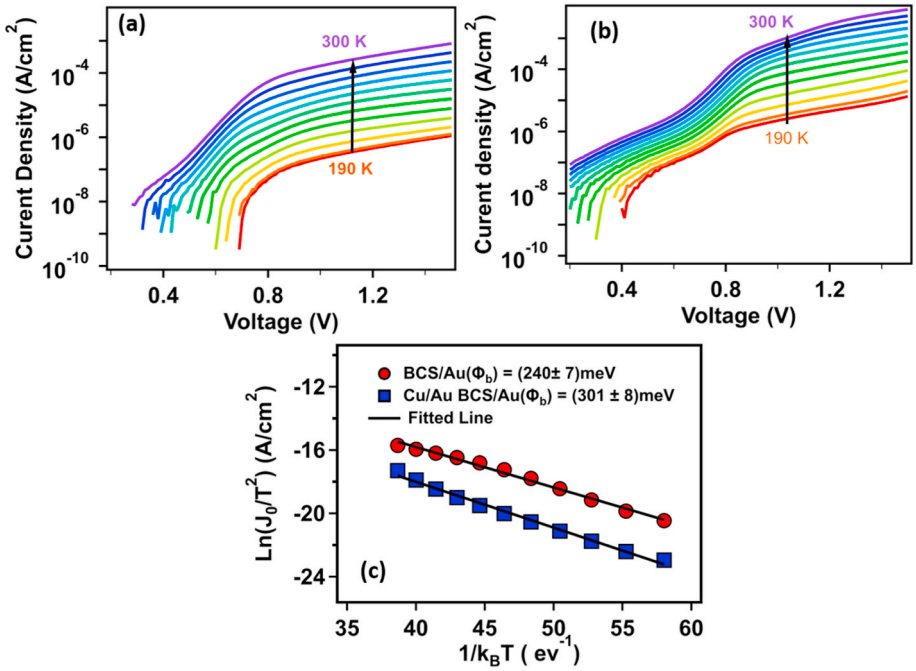

Fig. 7. J-V-T measurement of CdTe devices with (a) Cu/Au, (b) BCS/Au as a back buffer layer from 190 K to 300 K, and (c) plots of Ln (J_0/T^2) versus 1/k_BT (the solid lines represent the fitted line) and fitted values for BCS/Au and Cu/Au back contact on CdTe devices.

both proper band-bending and low interface recombination velocity.

Room temperature C–V measurements were carried out to estimate the doping concentration for CdTe devices with and without BCS interfacial layer as shown in Fig. 6. All the measurements were carried in the dark condition at the DC bias voltage (VDC) swept from −3 V to +1 V whereas AC modulation voltage of 45 mV rms and the frequency of 10 kHz is used. Carrier density of CdTe device completed with BCS/Au and Au is 1.11 × 10^{14} cm^{-3} and 1.13 × 10^{14} cm^{-3} respectively. This slight difference in the carrier density between these two devices may be due to the variation of device position (3″ × 3”). Although Cu atoms/ions are mobile, and they might diffuse to CdTe during the deposition and annealing of the BCS layer, the values of the doping density obtained from C–V measurements indicate that the BCS layer did not increase the free carrier concentration of CdTe devices even though post annealing treatment was done at 270 °C for 5 min.

Since BCS films not only worked as back contact layer but also does etching on the CdTe surface and makes Te rich surface. To calculate the back barrier height of CdTe device, temperature dependent current voltage (J-V-T) measurement was carried from 190 K to 300 K temperature range from −0.5 V to 1.5 V. Fig. 7(a) and (b) are J-V-T curves of CdTe/BCS/Au and CdTe/Cu/Au respectively. To calculate back barrier height of these devices, thermionic emission model is used as given by the equation,

$$J_0 \alpha T^2 \exp\left(-\frac{q\Phi_b}{k_B T}\right) \quad (2)$$

From Eq (2) back barrier height (Φ_b) is obtained by the slope of Arrhenius plots of Ln (J_0/T^2) versus 1/k_BT where k_B is the Boltzmann constant, q is electronic charge, and J_0 is the saturation current. From Fig. 7(c), the barrier height of the standard Cu/Au is about (301 ± 8) meV while for BCS/Au is (240 ± 7) meV. These values of back barrier height match closely with previous results for standard Cu/Au and etched CdTe devices using wet chemical etching process [23]. Due to the decrease in barrier height, it facilitates the hole transport towards the back electrode and reduces recombination at the back interface [55]. This decrease in the back barrier height supports the increase on the device performance with excellent improvement on V_{OC} and FF.

4. Conclusions

We have synthesized and studied the properties of BCS thin films prepared using a solution based approach; the films show high optical transmission (>70% at 400–900 nm wavelengths) and wide band gap energy (~1.92 eV). The test of BCS as a back-buffer layer in CdTe solar cells shows relative device performance increased by 7.5% for VTD deposited CdTe, and the results are the same if we use the CSS deposited CdTe, showing improvements in V_{OC}, *FF* in comparison to a control Cu/Au back contact design. A successful demonstration of using BCS thin films as back contacts in CdTe solar cells shows it could serve as a promising interface layer for the opaque and semitransparent CdTe PV by creating a Te-rich CdTe surface. From C–V and J-V-T measurement BCS does not help to increase the doping density of CdTe but helps to reduce the back barrier height. Furthermore, CdTe PV devices with BCS/ITO show promising performance, in a transparent back contact architecture, using ITO as back electrode layer.

Credit author statement

Kamala Khanal Subedi: Conceptualization, investigation, writing – original draft preparation. **Ebin Bastola**: Experimental and analytical support, writing – review and editing. **Indra Subedi**: investigation. **Sandip Bista**: investigation. **Suman Rijal**: investigation. **Manoj K. Jamarkattel**: Investigation, JVT measurements and analysis. **Rasha A. Awni**: Investigation, CV measurements and analysis. **Adam B. Philips**: writing – review and editing, supervision. **Yanfa Yan**: supervision, funding acquisition. **Michael J. Heben**: supervision, funding acquisition. **Nikolas J. Podraza**: supervision, funding acquisition. **Randy J. Ellingson**: writing – review and editing, supervision, project administration, funding acquisition.

Declaration of competing interest

The authors declare that they have no known competing financial interests or personal relationships that could have appeared to influence the work reported in this paper.

Acknowledgements

This material is based on research sponsored by Air Force Research Laboratory under agreement numbers FA9453-18-2-0037, FA9453-19-C-1002, and by the U.S. DOE's Office of Energy Efficiency and Renewable Energy (EERE) under Solar Energy Technologies Office (SETO) Agreement DE-EE0008974. The U.S. Government is authorized to reproduce and distribute reprints for Governmental purposes notwithstanding any copyright notation thereon. The views and conclusions contained herein are those of the authors and should not be interpreted as necessarily representing the official policies or endorsements, either expressed or implied, of Air Force Research Laboratory or the U.S. Government. The authors would like to thank Willard and Kelsey Solar Group for providing CdS/CdTe.

Appendix A. Supplementary data

Supplementary data to this article can be found online at https://doi.org/10.1016/j.solmat.2020.110764.

References

[1] A. Facchetti, T. Marks, Transparent Electronics: from Synthesis to Applications, John Wiley & Sons, 2010.
[2] K. Nomura, H. Ohta, A. Takagi, T. Kamiya, M. Hirano, H. Hosono, Room-temperature fabrication of transparent flexible thin-film transistors using amorphous oxide semiconductors, Nature 432 (2004) 488.
[3] O. Mryasov, A.J. Freeman, Electronic band structure of indium tin oxide and criteria for transparent conducting behavior, Phys. Rev. B 64 (2001) 233111.
[4] A. Alves, D. Gomes, J. Silva, G. Silva, Fluorine-doped tin oxide surfaces modified by self-assembled alkanethiols for thin-film devices, Appl. Surf. Sci. 279 (2013) 67–70.
[5] H. Kawazoe, M. Yasukawa, H. Hyodo, M. Kurita, H. Yanagi, H. Hosono, P-type electrical conduction in transparent thin films of $CuAlO_2$, Nature 389 (1997) 939.
[6] X. Xu, J. Bullock, L.T. Schelhas, E.Z. Stutz, J.J. Fonseca, M. Hettick, V.L. Pool, K. F. Tai, M.F. Toney, X. Fang, Chemical bath deposition of p-type transparent, highly conducting $(CuS)_x$:$(ZnS)_{1-x}$ nanocomposite thin films and fabrication of Si heterojunction solar cells, Nano Lett. 16 (2016) 1925–1932.
[7] K.K. Subedi, E. Bastola, I. Subedi, Z. Song, K.P. Bhandari, A.B. Phillips, N. J. Podraza, M.J. Heben, R.J. Ellingson, Nanocomposite $(CuS)_x(ZnS)_{1-x}$ thin film back contact for CdTe solar cells: toward a bifacial device, Sol. Energy Mater. Sol. Cell. 186 (2018) 227–235.
[8] K.K. Subedi, K.P. Bhandari, E. Bastola, R.J. Ellingson, 13% CdS/CdTe solar cell using a nanocomposite $(CuS)_x(ZnS)_{1-x}$ thin film hole transport layer, in: 2017 IEEE 44th Photovoltaic Specialist Conference (PVSC), IEEE, 2017, pp. 781–784.
[9] S. Park, D.A. Keszler, M.M. Valencia, R.L. Hoffman, J.P. Bender, J.F. Wager, Transparent p-type conducting $BaCu_2S_2$ films, Appl. Phys. Lett. 80 (2002) 4393–4394.
[10] Y. Wang, M. Liu, F. Huang, L. Chen, H. Li, X. Lin, W. Wang, Y. Xia, Solution-processed p-type transparent conducting $BaCu_2S_2$ thin film, Chem. Mater. 19 (2007) 3102–3104.
[11] Y. Han, S. Siol, Q. Zhang, A. Zakutayev, Optoelectronic properties of strontium and barium copper sulfides prepared by combinatorial sputtering, Chem. Mater. 29 (2017) 8239–8248.
[12] A. Zunger, Practical doping principles 83 (2003) 57–59.
[13] F.Q. Huang, M.L. Liu, C. Yang, Highly enhanced p-type electrical conduction in wide band gap $Cu_{1+x}Al_{1-x}S_2$ polycrystals, Sol. Energy Mater. Sol. Cell. 95 (2011) 2924–2927.
[14] P.-a. Zong, K. Kimata, Z. Li, P. Zhang, J. Liang, C. Wan, K. Koumoto, A p-type thermoelectric material $BaCu_4S_3$ with high electronic band degeneracy, J. Appl. Phys. 126 (2019), 025102.
[15] K. Khanal Subedi, E. Bastola, I. Subedi, A.B. Phillips, M.J. Heben, N.J. Podraza, R. J. Ellingson, Bifacial CdS/CdTe Solar Cell using Transparent Barium Copper Sulfide as a Hole Transport Layer, in: 2019 IEEE 46th Photovoltaic Specialists Conference (PVSC), IEEE, 2019, pp. 185–188.
[16] V. Alekseenko, A. Alekseenko, The abundances of chemical elements in urban soils, J. Geochem. Explor. 147 (2014) 245–249.
[17] H. Chou, A. Rohatgi, E. Thomas, S. Kamra, A. Bhat, Effects of Cu on CdTe/CdS heterojunction solar cells with Au/Cu contacts, J. Electrochem. Soc. 142 (1995) 254–259.
[18] F.K. Alfadhili, A.B. Phillips, G.K. Liyanage, J.M. Gibbs, M.K. Jamarkattel, M.J.J.M. A. Heben, Controlling band Alignment at the back interface of cadmium telluride solar cells using ZnTe and Te buffer, Layers 4 (2019) 913–919.
[19] J. Li, D.R. Diercks, T.R. Ohno, C.W. Warren, M.C. Lonergan, J.D. Beach, C. A. Wolden, Controlled activation of ZnTe: Cu contacted CdTe solar cells using rapid thermal processing, Sol. Energy Mater. Sol. Cell. 133 (2015) 208–215.
[20] M.-J. Zhang, Q. Lin, X. Yang, Z. Mei, J. Liang, Y. Lin, F. Pan, Novel P-type conductive semiconductor nanocrystalline film as the back electrode for high-performance thin film solar cells, Nano Lett. 16 (2016) 1218–1223.
[21] E. Bastola, K.P. Bhandari, I. Subedi, N.J. Podraza, R.J. Ellingson, Structural, optical, and hole transport properties of earth-abundant chalcopyrite ($CuFeS_2$) nanocrystals, MRS Communications 8 (2018) 970–978.
[22] S.C. Watthage, A.B. Phillips, G.K. Liyanage, Z. Song, J.M. Gibbs, F.K. Alfadhili, R. B. Alkhayat, R.H. Ahangharnejhad, Z.S. Almutawah, K.P. Bhandari, Selective Cd removal from CdTe for high-efficiency Te back-contact formation, Journal of Photovoltaics 8 (2018) 1125–1131.
[23] E. Bastola, F.K. Alfadhili, A.B. Phillips, M.J. Heben, R.J. Ellingson, Wet chemical etching of cadmium telluride photovoltaics for enhanced open-circuit voltage, fill factor, and power conversion efficiency, J. Mater. Res. 34 (2019) 3988–3997.
[24] A. Moore, T. Song, J. Sites, Improved CdTe Solar-Cell Performance with an Evaporated Te Layer before the Back Contact, MRS Adv. 2 (2017) 3195–3201.
[25] G.K. Liyanage, A.B. Phillips, F.K. Alfadhili, R.J. Ellingson, M.J. Heben, The role of back buffer layers and absorber properties for> 25% efficient CdTe solar cells, ACS Appl. Energy Mater. 2 (2019) 5419–5426.
[26] A.B. Phillips, K. Khanal Subedi, G.K. Liyanage, F.K. Alfadhili, R.J. Ellingson, M. J. Heben, Understanding and Advancing Bifacial Thin Film Solar Cells, ACS Appl. Energy Mater. (2020) 6072–6078, https://doi.org/10.1021/acsaem.0c00851.
[27] J. Sites, J. Pan, Strategies to increase CdTe solar-cell voltage, Thin Solid Films 515 (2007) 6099–6102.
[29] R.R. Khanal, A.B. Phillips, Z. Song, Y. Xie, H.P. Mahabaduge, M.D. Dorogi, S. Zafar, G.T. Faykosh, M.J. Heben, Substrate configuration, bifacial CdTe solar cells grown directly on transparent single wall carbon nanotube back contacts, Sol. Energy Mater. Sol. Cell. 157 (2016) 35–41.
[31] J. Pang, Y. Cai, Q. He, H. Wang, W. Jiang, J. He, T. Yu, W. Liu, Y. Zhang, Y. Sun, Preparation and characteristics of $MoSe_2$ interlayer in bifacial Cu(In, Ga)Se_2 solar cells, Physics Procedia 32 (2012) 372–378.
[32] R.C. Ropp, Encyclopedia of the Alkaline Earth Compounds, Newnes, 2012.
[33] D.F. Swinehart, The beer-lambert law, J. Chem. Educ. 39 (1962) 333.
[34] B. Johs, C. Herzinger, Quantifying the accuracy of ellipsometer systems, Phys. Status Solidi C 5 (2008) 1031–1035.
[35] R.W. Collins, A.S. Ferlauto, Optical physics of materials, in: H.G. Tompkins, E. A. Irene (Eds.), Handbook of Ellipsometry, William Andrew, Norwich, NY, 2005, pp. 93–235.
[36] V.D. Bruggeman, Berechnung verschiedener physikalischer Konstanten von heterogenen Substanzen. I. Dielektrizitätskonstanten und Leitfähigkeiten der Mischkörper aus isotropen substanzen, Ann. Phys. 416 (1935) 636–664.
[37] I. Subedi, K.P. Bhandari, R.J. Ellingson, N.J. Podraza, Near infrared to ultraviolet optical properties of bulk single crystal and nanocrystal thin film iron pyrite, Nanotechnology 27 (2016) 295702.
[38] M.M. Junda, N.J. Podraza, Optical properties of soda lime float glass from 3 mm to 148 nm (0.41 meV to 8.38 eV) by spectroscopic ellipsometry, Surf. Sci. Spectra 25 (2018), 016001.
[39] A. Crovetto, R. Chen, R.B. Ettlinger, A.C. Cazzaniga, J. Schou, C. Persson, O. Hansen, Dielectric function and double absorption onset of monoclinic Cu_2SnS_3: origin of experimental features explained by first-principles calculations, Sol. Energy Mater. Sol. Cell. 154 (2016) 121–129.
[40] E. Shaaban, N. Afify, A. El-Taher, Effect of film thickness on microstructure parameters and optical constants of CdTe thin films, J. Alloys Compd. 482 (2009) 400–404.
[41] B.J. Simonds, H.J. Meadows, S. Misra, C. Ferekides, P.J. Dale, M.A. Scarpulla, Laser processing for thin film chalcogenide photovoltaics: a review and prospectus, J. Photon. Energy 5 (2015), 050999.
[42] Z. Su, K. Sun, Z. Han, H. Cui, F. Liu, Y. Lai, J. Li, X. Hao, Y. Liu, M.A. Green, Fabrication of Cu_2ZnSnS_4 solar cells with 5.1% efficiency via thermal decomposition and reaction using a non-toxic sol–gel route, J. Mater. Chem. 2 (2014) 500–509.
[43] Z. Chen, K. Sun, Z. Su, F. Liu, D. Tang, H. Xiao, L. Shi, L. Jiang, X. Hao, Y. Lai, Solution-Processed trigonal Cu_2BaSnS_4 thin-film solar cells, ACS Appl. Energy Mater. 1 (2018) 3420–3427.
[44] I. Dharmadasa, O. Echendu, F. Fauzi, N. Abdul-Manaf, O. Olusola, H. Salim, M. Madugu, A. Ojo, Improvement of composition of CdTe thin films during heat treatment in the presence of $CdCl_2$, J. Mater. Sci. Mater. Electron. 28 (2017) 2343–2352.
[45] A. Jarkov, S. Bereznev, O. Volobujeva, R. Traksmaa, A. Tverjanovich, A. Öpik, E. Mellikov, Photo-assisted electrodeposition of polypyrrole back contact to CdS/CdTe solar cell structures, Thin Solid Films 535 (2013) 198–201.
[46] V. Kosyak, Y. Znamenshchykov, A. Čerškus, Y.P. Gnatenko, L. Grase, J. Vecstaudza, A. Medvids, A. Opanasyuk, G. Mezinskis, Composition dependence of structural and optical properties of $Cd_{1-x}Zn_xTe$ thick films obtained by the close-spaced sublimation, J. Alloys Compd. 682 (2016) 543–551.
[47] P. Amirtharaj, F.H. Pollak, Raman scattering study of the properties and removal of excess Te on CdTe surfaces, Appl. Phys. Lett. 45 (1984) 789–791.
[48] W.S. Rasband, Imagej, us, national institutes of health, bethesda, maryland, usa, 2011.
[49] C.A. Wolden, A. Abbas, J. Li, D.R. Diercks, D.M. Meysing, T.R. Ohno, J.D. Beach, T. M. Barnes, J.M. Walls, The roles of ZnTe buffer layers on CdTe solar cell performance, Sol. Energy Mater. Sol. Cells 147 (2016) 203–210.
[50] A.N. Tiwari, G. Khrypunov, F. Kurdzesau, D. Bätzner, A. Romeo, H. Zogg, CdTe solar cell in a novel configuration, Progress in Photovoltaics 12 (2004) 33–38.
[51] J. Zide, A. Kleiman-Shwarsctein, N. Strandwitz, J. Zimmerman, T. Steenblock-Smith, A. Gossard, A. Forman, A. Ivanovskaya, G. Stucky, Increased efficiency in multijunction solar cells through the incorporation of semimetallic ErAs nanoparticles into the tunnel junction, Appl. Phys. Lett. 88 (2006) 162103.
[52] B. Yu, F. Zhu, H. Wang, G. Li, D. Yan, All-organic tunnel junctions as connecting units in tandem organic solar cell, J. Appl. Phys. 104 (2008) 114503.

[53] M.J. Romero, T.A. Gessert, M.M. Al-Jassim, Carrier diffusion and radiative recombination in CdTe thin films, Appl. Phys. Lett. 81 (2002) 3161–3163.
[54] D. Kuciauskas, A. Kanevce, J.M. Burst, J.N. Duenow, R. Dhere, D.S. Albin, D. H. Levi, R.K. Ahrenkiel, Minority carrier lifetime analysis in the bulk of thin-film absorbers using subbandgap (two-photon) excitation, Journal of Photovoltaics 3 (2013) 1319–1324.
[55] R.A. Awni, D.B. Li, C.R. Grice, Z. Song, M.A. Razooqi, A.B. Phillips, S.S. Bista, P. J. Roland, F.K. Alfadhili, R.J. Ellingson, M.J. Heben, J.V. Li, Y. Yan, The effects of hydrogen iodide back surface treatment on CdTe solar cells, Solar RRL 3 (2019) 1800304.